Optimizing the Frequency Positioning of Tunable Couplers in a Circuit QED Processor to Mitigate Spectator Effects on Quantum Operations

S. Vallés-Sanclemente,[1] T. H. F. Vroomans,[1] T. R. van Abswoude,[2] T. Stavenga,[3] F. Brulleman,[3] S. L. M. van der Meer,[1] Y. Xin,[1] A. Lawrence,[2] V. Singh,[1,†] M. A. Rol,[2] and L. DiCarlo[1,*]

[1]QuTech and Kavli Institute of Nanoscience, Delft University of Technology, P.O. Box 5046, 2600 GA Delft, The Netherlands
[2]Orange Quantum Systems, Elektronicaweg 2, 2628 XG Delft, The Netherlands
[3]Quantware B.V., Elektronicaweg 10, 2628 XG Delft, The Netherlands

(Received 15 April 2025; accepted 2 April 2026; published 18 May 2026)

We experimentally optimize the frequency of flux-tunable couplers in a superconducting quantum processor to minimize the impact of spectator transmons during quantum operations (single-qubit gates, two-qubit gates, and readout) on other transmons. We adapt a popular transmonlike tunable-coupling element, achieving high-fidelity, low-leakage controlled-Z gates with unipolar, fast-adiabatic pulsing only on the coupler. We demonstrate the ability of the tunable coupler to null residual-ZZ coupling as well as exchange couplings in the one- and two-excitation manifolds. However, the nulling of these coherent interactions is not simultaneous, prompting the exploration of trade-offs. We present experiments pinpointing spectator effects on specific quantum operations. We also study the combined effect on the three types of operations using repeated quantum parity measurements.

DOI: 10.1103/wdfj-4nbt

Residual quantum interactions between qubits are a key source of crosstalk in multiqubit processors. In particular, spectator (i.e., inactive) qubits during single-qubit gates, two-qubit gates, and readout of other qubits can introduce state-dependent errors. In legacy circuit quantum electrodynamics (QED) processors employing transmons coupled via fixed-frequency resonators, a dominant residual interaction is ZZ coupling, which adds a Hamiltonian term

$$\delta H = \hbar \xi_{ZZ}^{ij} |1_i 1_j\rangle\langle 1_i 1_j|,$$

making the qubit transition frequency of transmon Q_i dependent on the state of Q_j and vice versa. Here, $\hbar$ is the reduced Planck constant, and numbers indicate the energy excitation level. It is not uncommon for the coupling strength $|\xi_{ZZ}|/(2\pi)$ to reach MHz level for some pairs [1] due to limited frequency targeting accuracy. Postfabrication frequency trimming methods have allowed for taming $|\xi_{ZZ}|/(2\pi)$ to the ~100 kHz range in many cases [2,3].

*Contact author: l.dicarlo@tudelft.nl

†Present address: A*STAR Quantum Innovation Centre, Institute of Materials Research and Engineering, Agency for Science, Technology and Research, 2 Fusionopolis Way, 08-03, Singapore, Republic of Singapore.

Exchange interactions in the one- and two-excitation manifolds are strong, adding Hamiltonian terms

$$\hbar J_1^{ij} |0_i 1_j\rangle\langle 1_i 0_j| + \text{H.c.},$$
$$\hbar J_2^{ij} |1_i 1_j\rangle\langle 0_i 2_j| + \text{H.c.},$$

with coupling strengths $J_{1,2}/(2\pi)$ typically at the 10 MHz level. Only large detuning $|\Delta| \gg J$ between the coupled levels limits their impact.

In recent years, significant effort has focused on the development of flux-tunable couplers to mitigate these quantum interactions, a crucial step in the pursuit of fault-tolerant quantum computing [4–20]. A popular approach uses flux-tunable transmonlike elements [21–36], with variants including floating [37–42] and grounded [43–52], also used in chiplet-linking configurations [53,54]. The largest quantum processors demonstrated to date also employ this tunable coupler [33,55]. A characteristic of this approach is that ξ_{ZZ}, J_1, and J_2 can all be nulled, provided that the coupled transmons lie in the straddling regime where the qubit ($|0\rangle - |1\rangle$) transition of one transmon is flanked by the qubit and leakage ($|1\rangle - |2\rangle$) transitions of the other. Crucially though, ξ_{ZZ}, J_1, and J_2 cannot be simultaneously nulled at a single coupler-frequency setting [47]. This constraint stems from the structure of the dressed energy levels in the one- and two-excitation manifolds. (See Supplemental Material [56] for a detailed discussion of how these quantities depend on the tunable-coupler frequency.) This fact motivates the question, What tunable coupler positioning is best to mitigate the impact of spectator transmons on the fidelity of quantum operations (readout and single- and two-qubit gates) performed on other transmons?.

In this Letter, we experimentally address this question using a 5-transmon prototype of our tunable-coupler-based processor architecture. [This 5-transmon processor is publicly available as the Tuna-5 backend on the Quantum Inspire platform [67] together with a 9-transmon processor (Tuna-9) using the same architecture.] After mapping out the dependence of ξ_{ZZ}, J_1, and J_2 on coupler frequency, we first find that spectator effects on single-qubit gates are strongly mitigated over a wide range of coupler positioning, spanning both $\xi_{ZZ} = 0$ and $J_1 = 0$, but not $J_2 = 0$. However, for readout, nulling J_1 or J_2 is advantageous: it avoids the excitation exchange activated by measurement-induced spectral overlap between transitions of coupled transmons. To also consider the impact of spectators on two-qubit gates, we first consider several options for realizing controlled-Z (CZ) gates, converging on unipolar, fast-adiabatic flux pulsing only on the tunable coupler, achieving CZ error $\epsilon_{\mathrm{CZ}} < 1\%$ with leakage $L_1 \approx 0.05\%$. Our final experiment studies the combined effect of spectators on readout and single- and two-qubit gates in a minimal setting relevant for quantum error correction (QEC): repeated weight-2 parity checks with a baseline error-detection probability of $\sim 12\%$. When repeatedly toggling a spectator, we observe that the detection probability is lowest with the coupler biased around $\xi_{ZZ} = 0$, minimizing spectator effects on CZ.

Our device consists of five flux-tunable transmon qubits in a starfish configuration, with central transmon Q_0 connected to four corner transmons (Q_1-Q_4) via dedicated, also flux-tunable couplers C_{0i}. (Please see Supplemental Material [56] for device parameters and performance characteristics.) This qubit count and connectivity is a common choice for prototyping quantum-hardware architectures intended for QEC [68–70]. Numerical simulations show that the targeted coupling strengths, $g_{\mathrm{qq}}/(2\pi) =$ 6 MHz and $g_{\mathrm{qc}}/(2\pi) = 70$ MHz [56], can null ξ_{ZZ} with the transmons in the so-called straddling regime and the coupler positioned $\sim$700 MHz above the qubit transition frequencies. Spectroscopy of the coupler at $\xi_{ZZ} = 0$ confirms this prediction [56]. In this device, we find all coupled transmon pairs in the straddling regime with all biased at their simultaneous sweet spot, making this the clear choice of bias point for transmons as it maximizes qubit coherence.

We start our Letter by mapping the dependence of ξ_{ZZ}, J_1, and J_2 on coupler bias frequency. Figure 1(a) shows example results for pair (Q_1, Q_0) (see Supplemental Material [56] for similar results for the other pairs). We measure ξ_{ZZ} using a modified echo sequence [71] and J_1 (J_2) by spectroscopy of the $|0_1 1_0\rangle - |1_1 0_0\rangle$ ($|1_1 1_0\rangle - |0_1 2_0\rangle$) avoided crossing reached by flux biasing Q_0 (Q_1) away from sweet spot. Decoherence limits the ability of

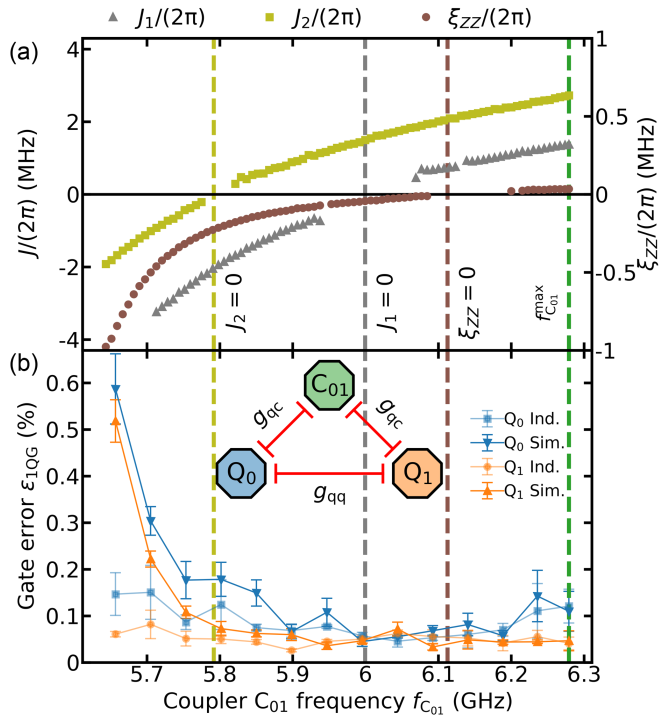

FIG. 1. Single-qubit gate performance as a function of tunable coupler frequency. (a) J_1, J_2, and ξ_{ZZ} between Q_1 and Q_0 as a function of coupler C_{01} frequency. Vertical gray, golden, and brown lines indicate the C_{01} frequencies at which J_1, J_2, and ξ_{ZZ} are nulled, respectively. (b) Single-qubit gate errors on Q_0 and Q_1, measured using simultaneous and individual randomized benchmarking, as a function of C_{01} frequency. Error bars are the standard deviation of the mean computed from 10 repetitions. Inset: schematic of the subsystem formed by Q_1, Q_0, and C_{01}. Q_1 and Q_0 are biased at their sweet spot frequencies of 5.218 and 5.295 GHz, respectively.

both methods to accurately extract these quantities at their zero crossings. When necessary, we rely on polynomial fits to exact the C_{01} frequencies at which they are nulled. The results clearly illustrate that the three interaction strengths can be nulled, but not simultaneously.

We first focus on single-qubit gates, studying the impact of C_{01} bias frequency on the individual and simultaneous single-qubit gate performance of Q_1 and Q_0 [Fig. 1(b)]. Individual single-qubit randomized benchmarking (RB) with the other transmon kept in $|0\rangle$ provides a baseline single-qubit native gate error $\lesssim 0.1\%$ across most of the 650 MHz range covered in C_{01}. We attribute the increase observed at the lower end of C_{01} frequency to increased transmon dephasing due to hybridization with the coupler and increased sensitivity of the bare coupler to $1/f$ flux noise [56]. Simultaneous performance matches individual performance over a wide C_{01} range, including $\xi_{ZZ}^{01} = 0$ and $J_1^{01} = 0$. A degradation is observed in simultaneous performance by $J_2 = 0$. Note that the C_{01} sweet spot limits our ability to extensively cover the $\xi_{ZZ}^{01} > 0$ regime. This is intentional: we strategically targeted couplers to have sweet spots just above $\xi_{ZZ}^{01} = 0$ to avoid unnecessarily compromising on their coherence.

During the above study, we observed that $\xi_{ZZ}^{01} = 0$ is not the optimal choice for readout. Specifically, at this C_{01} bias, we found it impossible to achieve an average assignment error [72] $\epsilon_{RO} < 2.5\%$ for Q_0, whose qubit transition frequency is above that of Q_1. The underlying physical reason is population exchange $|1_0 0_1\rangle \rightarrow |0_0 1_1\rangle$ activated during readout: photons injected to the Q_0 readout mode cause a Stark shift of Q_0, displacing its qubit transition downward in frequency and broadening its linewidth [73], causing spectral overlap with Q_1. Similar physics has been used to explain enhanced qubit relaxation during readout, caused by Stark-shift activated exchange with lower-frequency two-level defects [74]. Figure 2 evidences the phenomenon, showing the excitation exchange from Q_0 to

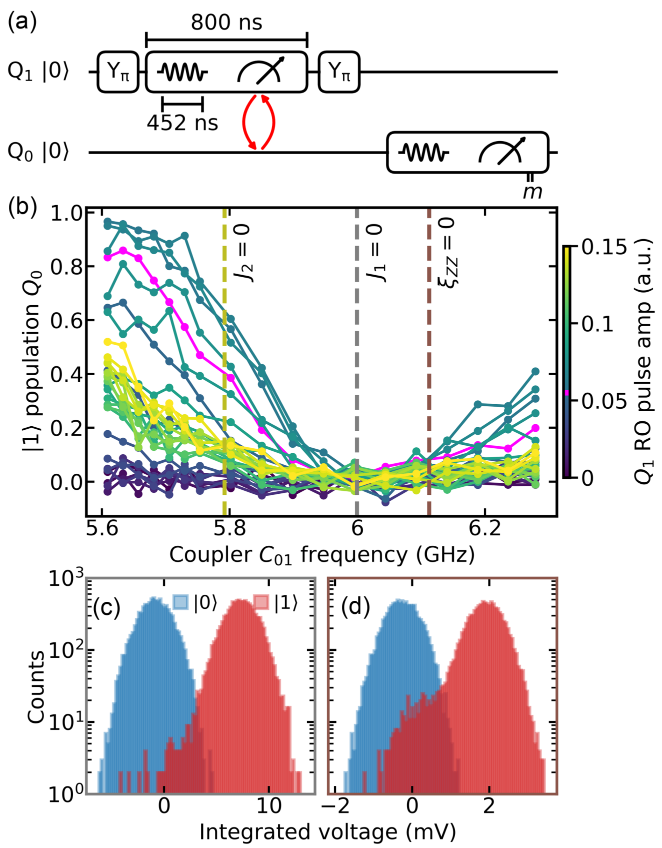

FIG. 2. Measurement-induced population exchange. (a) Schematic depicting a measurement pulse applied to Q_1 after preparing it in the excited state. This pulse is followed by a measurement of Q_0 to quantify the population exchange between the qubits. (b) Population of Q_1 as a function of C_{01} frequency and amplitude of the Q_0 readout pulse. The amplitude is expressed as a fraction of the maximum output of the Qblox QRM-RF module used for readout. The pink trace shows the data acquired with the chosen amplitude [56]. (c) Single-shot readout characterization for Q_0 at $J_1 = 0$, yielding $\epsilon_{RO} = 0.8\%$. (d) Similar characterization at $\xi_{ZZ} = 0$ and using identical readout parameters, yielding $\epsilon_{RO} = 2.5\%$.

Q_1 as a function of both Q_0 readout pulse amplitude and C_{01} bias. The detuning between qubits also plays a role, maximizing the exchange when it is comparable to the Stark-shift induced by the readout pulse [56]. Population exchange is strongly suppressed in a C_{01} frequency range centered around $J_1^{01} = 0$, where $\epsilon_{RO} < 1\%$ is reached for Q_0 with a total readout duration of 800 ns (including photon depletion). Remarkably, population exchange $|11\rangle \rightarrow |02\rangle$ may also occur during readout and can be mitigated at $J_2 = 0$ bias (see Supplemental Material [56] for a study of this effect), although this configuration is unattractive for single-qubit gates since it leads to $\xi_{ZZ}/(2\pi) > 1$ MHz. As all coupled transmon pairs have $\xi_{ZZ}/(2\pi) < 100$ kHz at $J_1 = 0$, and in consideration of Fig. 1, it seems tempting to choose this bias as the default for all couplers (see Supplemental Material [56] for a summary of the operating frequencies at this coupler bias). However, it remains important to also study spectator effects on two-qubit gates.

To this end, we must now choose an implementation of CZ gates drawing inspiration from prior work on similar tunable-coupling architectures [28,38,40,43,44,47] (Fig. 3). A general controlled-phase gate can be implemented by dynamically detuning the coupler, controllably increasing ξ_{ZZ} until the target conditional phase is acquired [28,43,44,52]. We study the conditional phase and missing fraction (a proxy for leakage) [75] of pair (Q_2, Q_0) in response to a unipolar, fast-adiabatic pulse [76] on C_{02} and a square pulse to the lower-frequency Q_2, both of duration 60 ns. The conditional-phase landscape displays a contour of 180°, the required phase for CZ. We select four points along this contour to evaluate the performance of CZ gates using interleaved RB with modifications to quantify leakage [77,78]. The best performance is achieved when Q_2 remains at the sweet spot (i.e., only the coupler is pulsed). Numerical simulations [56] show that the missing fraction here is mostly due to leakage to state $|1_{Q2} 1_{C02} 0_{Q0}\rangle$. Here, we extract a CZ gate error $\epsilon_{CZ} = (0.62 \pm 0.03)\%$ with leakage $L_1 = (0.051 \pm 0.014)\%$. Most likely, this choice maximizes fidelity because keeping Q_2 at sweet spot maximizes its coherence, as shown in Figs. 3(e) and 3(f). However, we did not perform detailed numerical simulation to dissect the contribution of different physical error sources to the error budget [71,75].

We can now study the combined effect of spectators on readout and single- and two-qubit gates in a minimal setting relevant for QEC [79]. Specifically, we perform repeated indirect measurements of the parity operator $X_2 X_1$ using Q_0 as ancilla and Q_4 as spectator (Fig. 4). We extract the error-detection probability for up to 100 rounds as a function of C_{04} bias frequency without and with toggling Q_4 between ground and first-excited state in every round (similar results are obtained when using Q_3 as the spectator [56]). The error-detection probability is a common metric in QEC to evaluate the performance of a parity

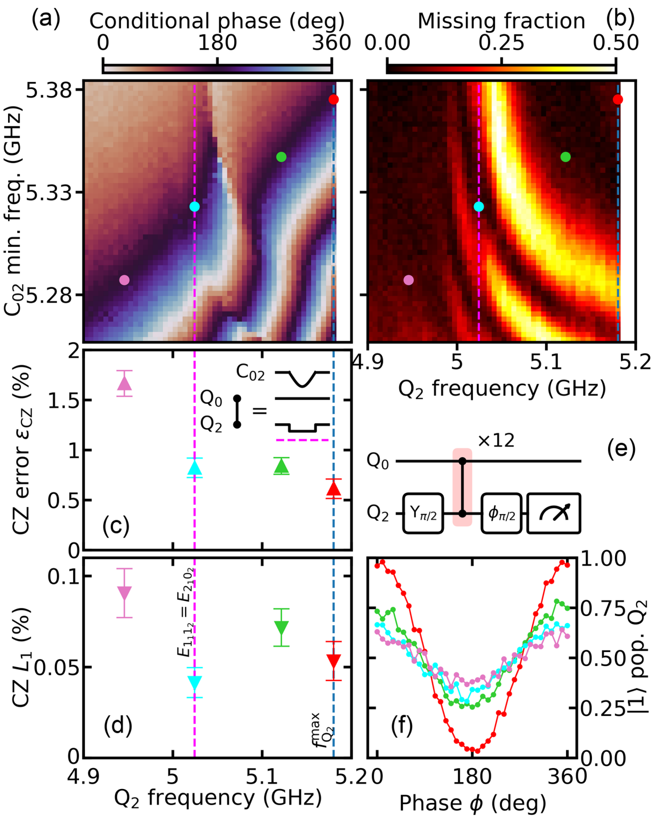

FIG. 3. Study of a CZ gate between Q_2 and Q_0, implemented by applying a fast-adiabatic flux pulse to coupler C_{02} and a square pulse to the lower-frequency qubit, Q_2. (a),(b) Conditional phase and missing fraction extracted from conditional oscillation experiments. (c),(d) CZ error and leakage measured using interleaved RB at four points along the contour of 180° conditional phase [colored markers in (a), (b)]. Error bars are the standard deviation of the mean computed from 5 repetitions. The inset in (c) is a cartoon representation of frequency excursions of C_{02}, Q_0, and Q_2. (e) Schematic of a Ramsey-like experiment that interleaves 12 CZ gates between two $\pi/2$ pulses, the last of which has phase ϕ. (f) Ramsey oscillations for the four chosen CZ settings, clearly showing that the impact on coherence is lowest when Q_2 remains at its sweet spot, as expected.

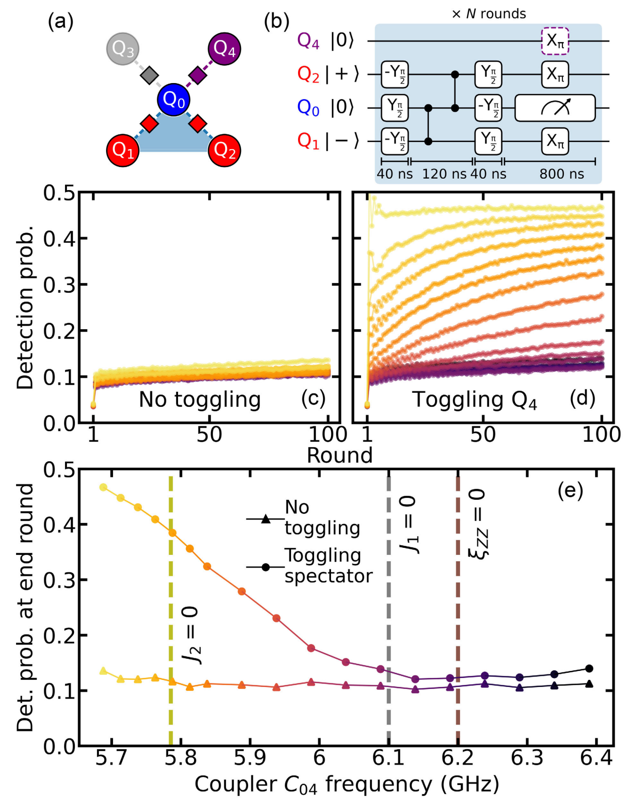

FIG. 4. Study of spectator effects during repeated parity checks. (a) Simplified schematic of the device with color coding to identify data qubits (Q_1 and Q_2, red), ancilla (Q_0, blue), and spectator (Q_4, purple). (b) Quantum circuit realizing the indirect measurement of X_2X_1 parity using Q_0 as ancilla. A X_π pulse is applied to Q_1 and Q_2 during readout of Q_0. To study spectator effects, a X_π pulse is applied to Q_4, toggling it between ground and first-excited state in every round. (c) Error-detection probability measured over 100 rounds at different C_{04} frequencies (represented by the color scale), keeping spectator Q_4 in the ground state. (d) Error-detection probability measured now toggling Q_4 at every round. (e) Common plot of the error-detection probability at round 100 for data in (c) and (d). Vertical lines mark the $\xi_{ZZ}^{04} = 0$, $J_1^{04} = 0$ and $J_2^{04} = 0$ coupler bias points.

check [27,31,33,55,80,81]. At a given round, it is defined as the fraction of times that the declared parity outcome does not match that declared in the previous round. For a weight-2 parity check (like in Fig. 4), toggling a spectator qubit can give a lower bound to the error-detection probability of a weight-4 parity check that would include all qubits in a larger QEC experiment. When Q_4 is not toggled, the error-detection probability is largely insensitive to C_{04} positioning, remaining $< 12\%$ over all bias positions and all rounds. This value is higher than the state-of-the-art $\sim 5\%$ [33]; we leave a more in-depth error budgeting of the parity-check performance as future work. By contrast, when Q_4 is toggled, the error-detection probability remains low and nearly round independent only near $\xi_{ZZ}^{04} = 0$. This suggests that spectator effects on CZ are minimized at $\xi_{ZZ} = 0$. A slight degradation is observed by $J_1^{04} = 0$ (more noticeable when toggling Q_3 instead of Q_4 [56]). As $|\xi_{ZZ}^{04}|$ further increases, the error-detection probability rises, showing a positive slope toward a higher steady state with increasing rounds. This slope is a hallmark of leakage [27,82] to higher-excited transmon states (of Q_0 in this case). Note that because the Q_0 qubit frequency is below that of Q_4, no measurement-induced exchange is expected to take place in the one-excitation manifold [56]. However, exchange can occur in the two-excitation manifold as $|1_4 1_0\rangle$ is Stark-shifted toward $|2_4, 0_0\rangle$ (In [56] we show that this effect is suppressed at the $J_2^{04} = 0$ bias.) This effect could underlie the small increase in error-detection probability at $\xi_{ZZ} = 0$ observed when toggling Q_4. An isolated study of spectator effects on the CZ gates played during the parity check shows that the conditional phase remains unaffected when toggling a spectator at any coupler bias, while errors on the single-qubit phase can only be avoided at the $\xi_{ZZ} = 0$ condition [56].

In summary, we have performed an experimental study to identify the best frequency positioning of flux-tunable, transmonlike couplers to mitigate spectator effects on quantum operations in a circuit QED processor. We show that this type of tunable coupler can null ZZ and exchange couplings, but not simultaneously. For single-qubit gates, spectator effects are minimized at a coupler bias region that spans $J_1 = 0$ and $\xi_{ZZ} = 0$. For two-qubit gates, the conditional phase remains mostly unaffected by spectator effects independently of coupler bias, while errors in the single-qubit phase updates can only be suppressed at $\xi_{ZZ} = 0$ [56]. This is also the preferable configuration at which spectator errors in a minimal multiqubit experiment are mitigated. For readout, however, spectator effects are minimized at $J_1 = 0$ ($J_2 = 0$ to measure state $|11\rangle$ [56]) when the detuning to the spectator transmon is comparable to the Stark shift introduced by the readout pulse. Consequently, it could prove beneficial to dynamically switch between nulling conditions for different quantum operations, taking advantage of the fast flux tunability already in place and calibrated for two-qubit gates. In [56], we present a proof of principle of this flux-assisted readout strategy, showing a clear decrease in average assignment error by dynamically tuning the coupler to $J_1 = 0$ during readout. Moving forward, it will also be important to further test our device architecture and spectator-effect mitigation strategies on larger devices, for example the 17-transmon, 24-coupler processor required for the distance-3 surface code [31,80,81], where all transmons couple to either two, three, or four nearest neighbors. It is also interesting to explore alternative tunable-coupling strategies with the capability to simultaneously null ZZ and exchange interactions [83].

Acknowledgments—We thank S. Dobrovolskiy and G. Limodio of QuantWare for fabricating the device; F. Battistel, A. Radhakrishnan, and R. Navarathna of Qblox for assistance with electronics; H. Ali and E. Y. Huang for insightful discussions; and V. Sinha for project management assistance. We are grateful to G. Calusine and W. Oliver for providing the traveling-wave parametric amplifier used in the amplification chain. This research is funded by the Netherlands Organization for Scientific Research (NWA.1292.19.194), Quantum Delta NL (DiagnostiQ and National Growth Fund KAT-1), the Allowance for Top Consortia for Knowledge and Innovation (TKI) of the Dutch Ministry of Economic Affairs, the European Union Flagship on Quantum Technology (OpenSuperQplus100, No. 101113946), and Intel Corporation.

S. V. S. and L. D. C. conceptualized the experimental study. S. V. S. performed the experiment with contributions from T. H. F. V., T. R. A., A. L., and M. A. R. S. V. S. performed the data analysis with contributions from T. H. F. V., S. L. M. M., and Y. X. S. V. S., T. H. F. V., and L. D. C. designed the Hamiltonian parameters of device, with contributions from V. S. T. S. and F. B. designed the device layout to target these parameters. T. S. performed the numerical simulations of the CZ gate. S. V. S. and L. D. C. wrote the manuscript with contributions from T. S. and F. B., with feedback from all coauthors. L. D. C. supervised the project.

Data availability—The data that support the findings of this article are openly available [84].

[1] J. F. Marques, B. M. Varbanov, M. S. Moreira, H. Ali, N. Muthusubramanian, C. Zachariadis, F. Battistel, M. Beekman, N. Haider, W. Vlothuizen, A. Bruno, B. M. Terhal, and L. DiCarlo, Nat. Phys. **18**, 80 (2022).
[2] E. J. Zhang *et al.*, Sci. Adv. **8**, eabi6690 (2022).
[3] D. P. Pappas, M. Field, C. J. Kopas, J. A. Howard, X. Wang, E. Lachman, J. Oh, L. Zhou, A. Gold, G. M. Stehl, K. Yadavalli, E. A. Sete, A. Bestwick, M. J. Kramer, and J. Y. Mutus, Commun. Mater. **5**, 150 (2024).
[4] T. Hime, P. A. Reichardt, B. L. T. Plourde, T. L. Roberson, C.-E. Wu, A. V. Ustinov, and J. Clarke, Science **314**, 1427 (2006).
[5] P. Bertet, C. J. P. M. Harmans, and J. E. Mooij, Phys. Rev. B **73**, 064512 (2006).
[6] A. O. Niskanen, K. Harrabi, F. Yoshihara, Y. Nakamura, S. Lloyd, and J. S. Tsai, Science **316**, 723 (2007).
[7] S. H. W. van der Ploeg, A. Izmalkov, A. M. van den Brink, U. Hübner, M. Grajcar, E. Il'ichev, H.-G. Meyer, and A. M. Zagoskin, Phys. Rev. Lett. **98**, 057004 (2007).
[8] R. Harris, A. J. Berkley, M. W. Johnson, P. Bunyk, S. Govorkov, M. C. Thom, S. Uchaikin, A. B. Wilson, J. Chung, E. Holtham, J. D. Biamonte, A. Y. Smirnov, M. H. S. Amin, and A. Maassenvandenbrink, Phys. Rev. Lett. **98**, 177001 (2007).
[9] M. S. Allman, F. Altomare, J. D. Whittaker, K. Cicak, D. Li, A. Sirois, J. Strong, J. D. Teufel, and R. W. Simmonds, Phys. Rev. Lett. **104**, 177004 (2010).
[10] R. C. Bialczak, M. Ansmann, M. Hofheinz, M. Lenander, E. Lucero, M. Neeley, A. O'Connell, D. Sank, H. Wang, M. Weides, J. Wenner, T. Yamamoto, A. N. Cleland, and J. M. Martinis, Phys. Rev. Lett. **106**, 060501 (2011).
[11] S. J. Srinivasan, A. J. Hoffman, J. M. Gambetta, and A. A. Houck, Phys. Rev. Lett. **106**, 083601 (2011).
[12] Y. Yin, Y. Chen, D. Sank, P. J. J. O'Malley, T. C. White, R. Barends, J. Kelly, E. Lucero, M. Mariantoni, A. Megrant, C. Neill, A. Vainsencher, J. Wenner, A. N. Korotkov, A. N. Cleland, and J. M. Martinis, Phys. Rev. Lett. **110**, 107001 (2013).

[13] B. Peropadre, D. Zueco, F. Wulschner, F. Deppe, A. Marx, R. Gross, and J. J. García-Ripoll, Phys. Rev. B **87**, 134504 (2013).
[14] I.-C. Hoi, A. F. Kockum, T. Palomaki, T. M. Stace, B. Fan, L. Tornberg, S. R. Sathyamoorthy, G. Johansson, P. Delsing, and C. M. Wilson, Phys. Rev. Lett. **111**, 053601 (2013).
[15] M. Pierre, I.-M. Svensson, S. Raman Sathyamoorthy, G. Johansson, and P. Delsing, Appl. Phys. Lett. **104**, 232604 (2014).
[16] Y. Chen, C. Neill, P. Roushan, N. Leung, M. Fang, R. Barends, J. Kelly *et al.*, Phys. Rev. Lett. **113**, 220502 (2014).
[17] D. C. McKay, S. Filipp, A. Mezzacapo, E. Magesan, J. M. Chow, and J. M. Gambetta, Phys. Rev. Appl. **6**, 064007 (2016).
[18] S. J. Weber, G. O. Samach, D. Hover, S. Gustavsson, D. K. Kim, A. Melville, D. Rosenberg, A. P. Sears, F. Yan, J. L. Yoder *et al.*, Phys. Rev. Appl. **8**, 014004 (2017).
[19] Y. Lu, S. Chakram, N. Leung, N. Earnest, R. K. Naik, Z. Huang, P. Groszkowski, E. Kapit, J. Koch, and D. I. Schuster, Phys. Rev. Lett. **119**, 150502 (2017).
[20] M. Kounalakis, C. Dickel, A. Bruno, N. K. Langford, and G. A. Steele, npj Quantum Inf. **4**, 1 (2018).
[21] J. Koch, T. M. Yu, J. Gambetta, A. A. Houck, D. I. Schuster, J. Majer, A. Blais, M. H. Devoret, S. M. Girvin, and R. J. Schoelkopf, Phys. Rev. A **76**, 042319 (2007).
[22] F. Yan, D. Campbell, P. Krantz, M. Kjaergaard, D. Kim, J. L. Yoder, D. Hover, A. Sears, A. J. Kerman, T. P. Orlando, S. Gustavsson, and W. D. Oliver, Phys. Rev. Lett. **120**, 260504 (2018).
[23] S. Rosenblum, Y. Y. Gao, P. Reinhold, C. Wang, C. J. Axline, L. Frunzio, S. M. Girvin, L. Jiang, M. Mirrahimi, M. H. Devoret *et al.*, Nat. Commun. **9**, 652 (2018).
[24] Y. Y. Gao, B. J. Lester, K. S. Chou, L. Frunzio, M. H. Devoret, L. Jiang, S. Girvin, and R. J. Schoelkopf, Nature (London) **566**, 509 (2019).
[25] F. Arute, K. Arya, R. Babbush, D. Bacon, J. C. Bardin, R. Barends, R. Biswas, S. Boixo, F. G. Brandao, D. A. Buell *et al.*, Nature (London) **574**, 505 (2019).
[26] B. Foxen, C. Neill, A. Dunsworth, P. Roushan, B. Chiaro, A. Megrant, J. Kelly, Z. Chen, K. Satzinger, R. Barends *et al.*, Phys. Rev. Lett. **125**, 120504 (2020).
[27] Google Quantum AI, Nature (London) **595**, 383 (2021).
[28] J. Stehlik, D. M. Zajac, D. L. Underwood, T. Phung, J. Blair, S. Carnevale, D. Klaus, G. A. Keefe, A. Carniol, M. Kumph, M. Steffen, and O. E. Dial, Phys. Rev. Lett. **127**, 080505 (2021).
[29] H. Goto, Phys. Rev. Appl. **18**, 034038 (2022).
[30] K. Kubo and H. Goto, Appl. Phys. Lett. **122**, 064001 (2023).
[31] Google Quantum AI, Nature (London) **614**, 676 (2023).
[32] K. Kubo, Y. Ho, and H. Goto, Phys. Rev. Appl. **22**, 024057 (2024).
[33] Google Quantum AI, Nature (London) **638**, 920 (2025).
[34] X. Zhang, X. Zhang, C. Chen, K. Tang, K. Yi, K. Luo, Z. Xie, Y. Chen, and T. Yan, Phys. Rev. Appl. **24**, 034003 (2025).
[35] R. Li, K. Kubo, Y. Ho, Z. Yan, S. Inoue, Y. Nakamura, and H. Goto, Phys. Rev. Appl. **23**, 064069 (2025).
[36] N. Mehta, J. D. Teoh, T. Noh, A. Agrawal, R. Chamberlain, T.-C. Chien, J. C. Curtis, B. H. Elfeky, S. Farzaneh, B. Gudlewski *et al.*, arXiv:2503.10935.
[37] P. Mundada, G. Zhang, T. Hazard, and A. Houck, Phys. Rev. Appl. **12**, 054023 (2019).
[38] E. A. Sete, A. Q. Chen, R. Manenti, S. Kulshreshtha, and S. Poletto, Phys. Rev. Appl. **15**, 064063 (2021).
[39] I. N. Moskalenko, I. A. Simakov, N. N. Abramov, A. A. Grigorev, D. O. Moskalev, A. A. Pishchimova, N. S. Smirnov, E. V. Zikiy, I. A. Rodionov, and I. S. Besedin, npj Quantum Inf. **8**, 130 (2022).
[40] F. Marxer, A. Vepsäläinen, S. W. Jolin, J. Tuorila, A. Landra, C. Ockeloen-Korppi, W. Liu, O. Ahonen, A. Auer, L. Belzane *et al.*, PRX Quantum **4**, 010314 (2023).
[41] H.-T. Liu *et al.*, Phys. Rev. Lett. **135**, 050602 (2025).
[42] F. Marxer, J. Mrożek, J. Andersson, L. Abdurakhimov, J. Adam, V. Bergholm, R. Beriwal, C. F. Chan, S. Dahl, S. R. Das *et al.*, arXiv:2508.16437.
[43] M. C. Collodo, J. Herrmann, N. Lacroix, C. K. Andersen, A. Remm, S. Lazar, J.-C. Besse, T. Walter, A. Wallraff, and C. Eichler, Phys. Rev. Lett. **125**, 240502 (2020).
[44] Y. Xu, J. Chu, J. Yuan, J. Qiu, Y. Zhou, L. Zhang, X. Tan, Y. Yu, S. Liu, J. Li, F. Yan, and D. Yu, Phys. Rev. Lett. **125**, 240503 (2020).
[45] X. Li, T. Cai, H. Yan, Z. Wang, X. Pan, Y. Ma, W. Cai, J. Han, Z. Hua, X. Han, Y. Wu, H. Zhang, H. Wang, Y. Song, L. Duan, and L. Sun, Phys. Rev. Appl. **14**, 024070 (2020).
[46] X. Y. Han, T. Q. Cai, X. G. Li, Y. K. Wu, Y. W. Ma, Y. L. Ma, J. H. Wang, H. Y. Zhang, Y. P. Song, and L. M. Duan, Phys. Rev. A **102**, 022619 (2020).
[47] Y. Sung, L. Ding, J. Braumüller, A. Vepsäläinen, B. Kannan, M. Kjaergaard, A. Greene, G. O. Samach, C. McNally, D. Kim, A. Melville, B. M. Niedzielski, M. E. Schwartz, J. L. Yoder, T. P. Orlando, S. Gustavsson, and W. D. Oliver, Phys. Rev. X **11**, 021058 (2021).
[48] E. A. Sete, N. Didier, A. Q. Chen, S. Kulshreshtha, R. Manenti, and S. Poletto, Phys. Rev. Appl. **16**, 024050 (2021).
[49] Y. Ye, S. Cao, Y. Wu, X. Chen, Q. Zhu, S. Li, F. Chen, M. Gong, C. Zha, H.-L. Huang *et al.*, Chin. Phys. Lett. **38**, 100301 (2021).
[50] L. Ding, M. Hays, Y. Sung, B. Kannan, J. An, A. Di Paolo, A. H. Karamlou, T. M. Hazard, K. Azar, D. K. Kim, B. M. Niedzielski, A. Melville, M. E. Schwartz, J. L. Yoder, T. P. Orlando, S. Gustavsson, J. A. Grover, K. Serniak, and W. D. Oliver, Phys. Rev. X **13**, 031035 (2023).
[51] C. Križan, J. Biznárová, L. Chen, E. Hogedal, A. Osman, C. W. Warren, S. Kosen, H.-X. Li, T. Abad, A. Aggarwal *et al.*, New J. Phys. **27**, 074507 (2025).
[52] N. J. Glaser, F. A. Roy, I. Tsitsilin, L. Koch, N. Bruckmoser, J. Schirk, J. H. Romeiro, G. B. P. Huber, F. Wallner, M. Singh *et al.*, Phys. Rev. Appl. **24**, 024048 (2025).
[53] P. Zhao, Y. Zhang, G. Xue, Y. Jin, and H. Yu, Appl. Phys. Lett. **121**, 032601 (2022).
[54] D. L. Campbell, A. Kamal, L. Ranzani, M. Senatore, and M. D. LaHaye, Phys. Rev. Appl. **19**, 064043 (2023).
[55] L. Caune, L. Skoric, N. S. Blunt, A. Ruban, J. McDaniel, J. A. Valery, A. D. Patterson, A. V. Gramolin, J. Majaniemi, K. M. Barnes *et al.*, arXiv:2410.05202.

[56] See Supplemental Material at http://link.aps.org/supplemental/10.1103/wdfj-4nbt for additional information supporting statements and claims made in the main text, which includes Refs. [57–66].

[57] J. Heinsoo, C. K. Andersen, A. Remm, S. Krinner, T. Walter, Y. Salathé, S. Gasparinetti, J.-C. Besse, A. Potočnik, A. Wallraff, and C. Eichler, Phys. Rev. Appl. **10**, 034040 (2018).

[58] S. Vallés-Sanclemente, S. L. M. van der Meer, M. Finkel, N. Muthusubramanian, M. Beekman, H. Ali, J. F. Marques, C. Zachariadis, H. M. Veen, T. Stavenga, N. Haider, and L. DiCarlo, Appl. Phys. Lett. **123**, 034004 (2023).

[59] C. Macklin, K. O'brien, D. Hover, M. Schwartz, V. Bolkhovsky, X. Zhang, W. Oliver, and I. Siddiqi, Science **350**, 307 (2015).

[60] J. Braumüller, L. Ding, A. P. Vepsäläinen, Y. Sung, M. Kjaergaard, T. Menke, R. Winik, D. Kim, B. M. Niedzielski, A. Melville, J. L. Yoder, C. F. Hirjibehedin, T. P. Orlando, S. Gustavsson, and W. D. Oliver, Phys. Rev. Appl. **13**, 054079 (2020).

[61] C. Zhang, T.-L. Wang, L.-L. Guo, X.-Y. Yang, X.-X. Yang, P. Duan, Z.-L. Jia, W.-C. Kong, and G.-P. Guo, Appl. Phys. Lett. **122**, 024001 (2023).

[62] M. A. Rol, L. Ciorciaro, F. K. Malinowski, B. M. Tarasinski, R. E. Sagastizabal, C. C. Bultink, Y. Salathe, N. Haandbaek, J. Sedivy, and L. DiCarlo, Appl. Phys. Lett. **116**, 054001 (2020).

[63] C. Hellings, N. Lacroix, A. Remm, R. Boell, J. Herrmann, S. Lazăr, S. Krinner, F. Swiadek, C. K. Andersen, C. Eichler, and A. Wallraff, arXiv:2503.04610.

[64] C. C. Bultink, M. A. Rol, T. E. O'Brien, X. Fu, B. C. S. Dikken, C. Dickel, R. F. L. Vermeulen, J. C. de Sterke, A. Bruno, R. N. Schouten, and L. DiCarlo, Phys. Rev. Appl. **6**, 034008 (2016).

[65] E. Magesan, J. M. Gambetta, A. D. Córcoles, and J. M. Chow, Phys. Rev. Lett. **114**, 200501 (2015).

[66] C. A. Ryan, B. R. Johnson, J. M. Gambetta, J. M. Chow, M. P. da Silva, O. E. Dial, and T. A. Ohki, Phys. Rev. A **91**, 022118 (2015).

[67] Quantum Inspire website: https://www.quantum-inspire.com/.

[68] J. F. Marques, M. Moreira, A. Chapple, O. Benhayoune Khadraoui, B. Varbanov, A. McDonald, W. Banner, G. Cutter, M. Hays, H. Zhang, K. Nesterov, Y. Sung, M. Gingras, J. Knecht, B. Niedzielski, H. Stickler, M. Schwartz, A. Blais, K. Serniak, J. Grover, and W. Oliver, A fluxonium architecture for QEC, Part 2: Extensible and spectator-error-free two-qubit gate scheme, in APS Global Summit 2025 (American Physical Society, Anaheim, CA, 2025), MAR-J18/11.

[69] T. Noh, N. Mehta, J. Teoh, K. Chow, P. Lu, G. Liu, T. Keen, J. Yuan, S. Mundhada, J. Aumentado, S. H. Moseley, and R. Schoelkopf, Error-detected entangling gate operations between dual-rail cavity cavity qubit—Part 1, in *APS Global Summit 2025* (American Physical Society, Anaheim, CA, 2025), MAR-L17/2.

[70] N. Mehta, T. Noh, J. Teoh, K. Chow, P. Lu, G. Liu, T. Keen, J. Yuan, S. Mundhada, J. Aumentado, S. H. Moseley, and R. Schoelkopf, Error-detected entangling gate operations between dual-rail cavity cavity qubit—Part 2, in *APS Global Summit 2025* (American Physical Society, Anaheim, CA, 2025), MAR-L17/3.

[71] V. Negîrneac, H. Ali, N. Muthusubramanian, F. Battistel, R. Sagastizabal, M. S. Moreira, J. F. Marques, W. J. Vlothuizen, M. Beekman, C. Zachariadis, N. Haider, A. Bruno, and L. DiCarlo, Phys. Rev. Lett. **126**, 220502 (2021).

[72] E. H. Chen, T. J. Yoder, Y. Kim, N. Sundaresan, S. Srinivasan, M. Li, A. D. Corcoles, A. W. Cross, and M. Takita, Phys. Rev. Lett. **128**, 110504 (2022).

[73] D. I. Schuster, A. Wallraff, A. Blais, L. Frunzio, R.-S. Huang, J. Majer, S. M. Girvin, and R. J. Schoelkopf, Phys. Rev. Lett. **94**, 123602 (2005).

[74] T. Thorbeck, Z. Xiao, A. Kamal, and Luke C. Govia, Phys. Rev. Lett. **132**, 090602 (2024).

[75] M. A. Rol, F. Battistel, F. K. Malinowski, C. C. Bultink, B. M. Tarasinski, R. Vollmer, N. Haider, N. Muthusubramanian, A. Bruno, B. M. Terhal, and L. DiCarlo, Phys. Rev. Lett. **123**, 120502 (2019).

[76] J. M. Martinis and M. R. Geller, Phys. Rev. A **90**, 022307 (2014).

[77] E. Magesan, J. M. Gambetta, and J. Emerson, Phys. Rev. A **85**, 042311 (2012).

[78] C. J. Wood and J. M. Gambetta, Phys. Rev. A **97**, 032306 (2018).

[79] A. G. Fowler, M. Mariantoni, J. M. Martinis, and A. N. Cleland, Phys. Rev. A **86**, 032324 (2012).

[80] S. Krinner, N. Lacroix, A. Remm, A. Di Paolo, E. Genois, C. Leroux *et al.*, Nature (London) **605**, 669 (2022).

[81] I. Besedin, M. Kerschbaum, J. Knoll, I. Hesner, L. Bödeker, L. Colmenarez, L. Hofele, N. Lacroix, C. Hellings, F. Swiadek *et al.*, Nat. Phys. **22**, 189 (2026).

[82] M. McEwen, D. Kafri, Z. Chen, J. Atalaya, K. Satzinger, C. Quintana, P. V. Klimov, D. Sank, C. Gidney, A. Fowler *et al.*, Nat. Commun. **12**, 1761 (2021).

[83] L. Heunisch, C. Eichler, and M. J. Hartmann, Phys. Rev. Appl. **20**, 064037 (2023).

[84] S. Vallés-Sanclemente, T. H. F. Vroomans, T. R. van Abswoude, T. Stavenga, F. Brulleman, S. L. M. van der Meer, Y. Xin, A. Lawrence, V. Singh, M. A. Rol, and L. DiCarlo, SpectatorEffectsTunableCouplers (2025), https://github.com/DiCarloLab-Delft/SpectatorEffectsTunableCouplers.